The unidirectional emptying box

C. J. COFFEY AND G. R. HUNT†

Department of Civil and Environmental Engineering, Imperial College London, London SW7 2AZ, UK

A theoretical description of the turbulent mixing within and the draining of a dense fluid layer from a box connected to a uniform density, quiescent environment through openings in the top and the base of the box is presented in this paper. This is an extension of the draining model developed by Linden *et al.* (*Annu. Rev. Fluid Mech.* vol. 31, 1990, pp. 201–238) and includes terms that describe localized mixing within the emptying box at the density interface. Mixing is induced by a turbulent flow of replacement fluid into the box and as a consequence we predict, and observe in complementary experiments, the development of a three-layer stratification. Based on the data collated from previous researchers, three distinct formulations for entrainment fluxes across density interfaces are used to account for this localized mixing. The model was then solved numerically for the three mixing formulations. Analytical solutions were developed for one formulation directly and for a second on assuming that localized mixing is relatively weak though still significant in redistributing buoyancy on the timescale of the draining process. Comparisons between our theoretical predictions and the experimental data, which we have collected on the developing layer depths and their densities show good agreement. The differences in predictions between the three mixing formulations suggest that the normalized flux turbulently entrained across a density interface tends to a constant value for large values of a Froude number Fr_T, based on conditions of the inflow through the top of the box, and scales as the cube of Fr_T for small values of Fr_T. The upper limit on the rate of entrainment into the mixed layer results in a minimum time (t_D) to remove the original dense layer. Using our analytical solutions, we bound this time and show that $0.2t_E \lesssim t_D \lesssim t_E$, i.e. the original dense layer may be depleted up to five times more rapidly than when there is no internal mixing and the box empties in a time t_E.

Key words: mixing and dispersion, stratified flows, turbulent mixing

1. Introduction

We consider the 'emptying-box' problem, that is the draining of a dense fluid layer, under gravity, from a box connected to a less dense external environment via a combination of openings in the top and base of the box. The density difference between the dense fluid layer and stationary unstratified ambient is small compared with the ambient density, and the two fluids are miscible. Figure 1 shows a schematic of the box with (*a*) the initial two-layer stratification considered and (*b*) the typical three-layer flow established during the flushing, i.e. following the opening of the vents.

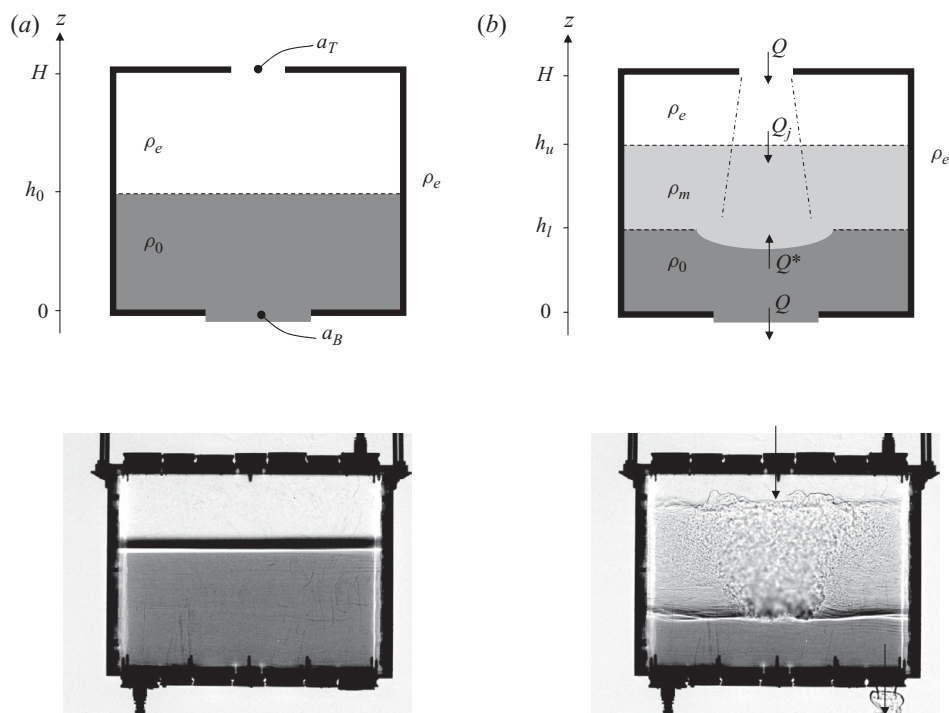† Email address for correspondence: gary.hunt@imperial.ac.uk

FIGURE 1. Schematics (upper panels) and associated shadowgraph images (lower panels) of a typical emptying-box flow ($R = 0.36$, $\lambda_T = 0.14$ and $\xi_0 = 0.62$, see (1.1)). (*a*) Initial conditions ($t = 0$) – a layer of dense fluid (density ρ_0, shown grey) below a layer at ambient density ρ_e (shown white). (*b*) The basic three-layer stratification observed for $t > 0$. The arrows indicate the volume fluxes in to and out of each of the three layers and the direction of flow through the openings. Localized turbulent mixing by the inflow is clearly evident in the shadowgraph at the lower density interface.

The main question, we address is how does the stratification within the emptying box develop.

Linden, Lane-Serff & Smeed (1990) presented an analytical model allowing the developing stratification to be predicted. Their model has provided a benchmark and starting point for numerous subsequent studies (see Linden 1999, for a review) and is applicable to initial conditions that result in minimal, or an absence of, mixing between the inflowing fluid at ambient density and the dense layer within the box so that the basic two-layer stratification is maintained throughout the draining period. As such their work is applicable to the purging of heat at night by (idealized) displacement ventilation from rooms or buildings in which the inflow of replacement air at low-level displaces, but does not mix with, warmer internal air. Linden *et al.* (1990) restricted their attention to horizontally oriented vents and we retain this orientation herein to enable direct comparison. Full-scale thermal measurements in rooms (Etheridge & Sandberg 1984) indicate that the developing stratification is somewhat more smeared than the stratification Linden *et al.* (1990) assumed and the physical grounds for this form is a focus of this study. They attribute the smearing to the effects of thermal diffusion and radiation.

The Reynolds and Péclet numbers for the night purging of heat from rooms are estimated to be $O(10^3)$–$O(10^4)$ and $O(10^2)$–$O(10^3)$, respectively (Etheridge &

Sandberg 1984). Over the time scale of a typical purge, i.e. a few hours, thermal diffusion for these high Péclet number flows does not provide the dominant mechanism for the redistribution of buoyancy. Generally, we have observed on opening the top and base vents in our experiments (a vertical inversion of the heated building example) that localized turbulent mixing, driven by a jet-like inflow of replacement fluid, occurs at the density interface causing dense fluid to be raised upwards (figure 1b). This mixed fluid forms an intermediate or mixed layer that deepens to fill the box (Hunt & Coffey 2010) rather than simply draining from the box. Turbulent mixing associated with a high Reynolds number jet-like flow of replacement air into a room is therefore likely to play a significant role in redistributing buoyancy and whilst a redistribution of heat in a room is not expected to dramatically alter the instantaneous rate of draining it would, for example, influence the comfort of occupants and impact on the efficiency of heat removal (Coffey & Hunt 2007).

The establishment, by a turbulent inflowing jet, and subsequent development of an intermediate layer as observed in our experiments are used herein to explain some of the differences between stratifications measured in rooms and the idealized displacement flow predictions of Linden *et al.* (1990). Whilst the orientation of openings in a room may not always be horizontal, many being vertically oriented, we anticipate that it is mixing induced by the inflow, rather than, for example, diffusion that is primarily responsible for the redistribution of buoyancy and the departure from a two-layer stratification.

Herein, we extend the Linden *et al.* (1990) model so that it may be applied across a wider range of initial conditions and geometries for which interfacial mixing significantly alters the form of the original two-layer stratification. Specifically, we develop a predictive model that may be applied to general emptying-box flows for which the direction of flow through both top and base openings remains constant and in one sense, i.e. so-called 'unidirectional' emptying-box flows (Hunt & Coffey 2010). This new model includes terms to account for mixing within the box due to the inflow through the top. By extending the Linden *et al.* (1990) model in this way, we are able to explore how mixing alters the form of the developing stratification and how the time taken to drain the original dense fluid layer is altered.

In the context of the primary application, namely, the passive night purging of heat from a room, it may be advantageous to induce mixing by the inflow on particularly cold evenings, and on warmer evenings to select a distribution and size of openings that inhibit the onset of mixing. In the absence of mixing, internal temperatures would fall as low as those in the external environment and potentially result in an overly cooled room at the start the following day. In contrast, avoiding mixing on warmer evenings and thereby flushing heat without diluting enhances the potential for cooling. Besides building ventilation, the work we developed has a potentially wider impact as the turbulent entrainment of fluid across density interfaces is of interest across a range of problems encountered in the natural environment, especially in geophysical fluid dynamics (Fernando & Smith 2001). Examples include atmospheric inversions eroded by buoyant plumes (Willis & Deardorff 1981, 1983, 1987; Presley & Telford 1988; Park, Seo & Lee 2001) and the ocean mixed layer deepening by cool or salty plumes (Thorpe 2005).

Hunt & Coffey (2010) identified, through a series of experiments, the initial conditions which lead to unidirectional flow through openings and which lead to bidirectional flow. We considered a box of height H and cross-sectional area S that connected to a quiescent external environment through circular openings in the top and base of areas a_T and a_B, respectively. The box initially contained a two-layer
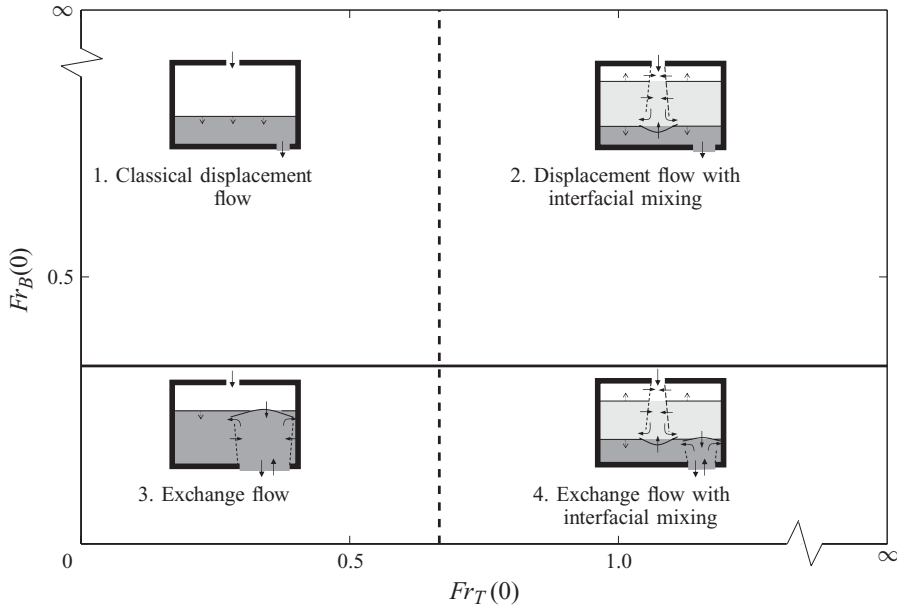
FIGURE 2. Plot of $\{Fr_T(0), Fr_B(0)\}$-space indicating four different draining behaviours. To the right of the vertical dotted line showing $Fr_T(0) = 0.67$ an intermediate or middle layer develops due to the interfacial mixing induced by inflow through the top. Above the horizontal line showing $Fr_B(0) = 0.33$, purely unidirectional flow occurs through the base and top (Hunt & Coffey 2010) – below this line, bidirectional flow is observed at the base. (Inset) Schematics highlighting the key features of each flow pattern.

stratification with a dense-layer depth h_0 as shown in figure 1(a). We showed that the development of the stratification and the direction of flow through the openings can be parameterized using three geometric ratios:

$$R = \frac{a_T}{a_B}, \quad \lambda_T = \frac{\sqrt{a_T}}{h_0} \quad \text{and} \quad \xi_0 = \frac{h_0}{H}, \tag{1.1}$$

where λ_T is a Richardson number relating an initial buoyancy-induced velocity to the initial velocity through the top opening. Two Froude numbers were formed from these ratios. The first, $Fr_T(0)$, characterizing the vigour of interfacial mixing driven by the inflow through the top:

$$Fr_T(0) = 2^{1/2} \frac{\alpha_{jet}}{\beta_{jet}^{1/2}} \frac{\lambda_T}{R} \left(\frac{1}{c_B^2} + \frac{1}{c_T^2 R^2} \right)^{-1/2} \left(\frac{1}{\xi_0} - 1 + \hat{z}_v \right)^{-3/2}, \tag{1.2a}$$

where $\alpha_{jet} = 7.0$ and $\beta_{jet} = 0.107$ are empirical constants, c_T and c_B are loss coefficients (≈ 0.6) and $\hat{z}_v = z_v / h_0 = \lambda_T / 0.107 \pi^{1/2}$ is an origin correction, and a second, $Fr_B(0)$, based on initial conditions at the base and characterizing whether a unidirectional outflow or a bidirectional flow occurs at the base:

$$Fr_B(0) = 2^{1/2} \lambda_T^{-1/2} R^{1/4} \left(\frac{1}{c_B^2} + \frac{1}{c_T^2 R^2} \right)^{-1/2}. \tag{1.2b}$$

Figure 2 shows how the $\{Fr_T(0), Fr_B(0)\}$-space divides into four regions, each region with a distinct emptying behaviour as indicated by the inset schematics.

We focus on the flows established within the region of $\{Fr_T(0), Fr_B(0)\}$-space above the horizontal line. For these unidirectional flows, replacement fluid enters solely through the top and dense fluid drains out through the base. The region of parameter space considered $(Fr_T(0) \gtrsim 0.67, Fr_B(0) \gtrsim 0.33)$ is readily achieved in naturally ventilated buildings, see §6. In fact, in the experiments we performed, the resulting class of emptying-box flow was relatively straightforward to achieve in contrast to idealized displacement flow – the latter required more extreme geometry ($R \ll 1$) and shallow initial dense-layer depths ξ_0.

In §2, we develop a theoretical model for predicting the time-dependent stratification and present analytical solutions (§4) for two special cases. The model is subsequently validated against measurements made in our laboratory experiments (§§3 and 4). Based on these results, we comment on the choice of formulation for entrainment fluxes across density interfaces (§5.1). Finally, we examine the time taken to deplete all fluid of the initial density ρ_0 (§5.2) – in other words, the time for the original dense fluid to drain from, or be mixed within, the interior so that no fluid of density ρ_0 remains thereafter.

2. Model development

The Linden *et al.* (1990) model is extended under the assumption that the stratification for $t > 0$ consists of three layers. This differs from the original Linden *et al.* (1990) model where two layers of uniform (and of the initial) density are assumed to persist. The basic three-layer stratification can clearly be seen in the shadowgraph image (figure 1*b*) and our assumption of three layers is consistent with quantitative measurements of $g'(z, t)$ made by Hunt & Coffey (2010) – the instantaneous reduced gravity at a height z defined by $g'(z) = g(\rho(z) - \rho_e)/\rho_e$, where g is the acceleration due to gravity and $\rho(z)$ the density of fluid in the box at height z. The assumed stratification (figure 1*b*) thus consists of a lower layer of depth $h_l(t)$ and uniform density $\rho_l(t) \equiv \rho_0$, a middle layer of depth $h_u(t) - h_l(t)$ and uniform density $\rho_m(t)$, and an upper layer of depth $H - h_u(t)$ and uniform density $\rho_u(t) \equiv \rho_e$. Following Linden *et al.* (1990), we focus on an insulated box so that there are no buoyancy transfers between the boundaries and the fluid.

On opening the vents at $t = 0$, our observations confirm that an inflowing turbulent jet at ambient density impinges on the density interface. This causes localized mixing and fluid to be raised from the lower layer, and which subsequently spreads along the interface as an intrusive gravity current, thereby forming a middle layer. The middle layer is assumed to form rapidly compared with the overall time scale of the draining process such that, at $t = 0$, the middle layer can be treated as infinitesimally thin. This is consistent with approaches by other researchers, e.g. Baines & Turner (1969) and Cardoso & Woods (1993), and with our experimental observations in which the formation of the middle layer took 1%–2% of the time taken to empty the box t_E, with that initial stratification and effective opening area, in the absence of mixing, see Linden *et al.* (1990) and §2.2.

Attention is restricted to geometries with $S \gg \{a_T, a_B\}$ and to cases where the characteristic Reynolds numbers ($Re_T = \sqrt{a_T g_0' h_0}/\nu$, $Re_B = \sqrt{a_B g_0' h_0}/\nu$, where ν is the kinematic viscosity) for flow through the openings are large. Reynolds numbers were typically of the order 10^4 and Péclet numbers of the order 10^6 in our experiments. Additionally, our model is developed for a single circular inlet opening. No restrictions are placed on the number of outlet openings.

2.1. *Conservation equations for the layers*

There is a net volume flux out of the lower layer ($0 \leqslant z \leqslant h_l$, figure 1*b*) due to the outward flux through the base, Q, and due to the turbulent flux entrained into the (middle) layer above at a rate Q^*. Thus, volume conservation for the lower layer requires

$$S\frac{\mathrm{d}h_l}{\mathrm{d}t} = -(Q + Q^*). \tag{2.1a}$$

For the middle layer ($h_l \leqslant z \leqslant h_u$), there is a volume flux Q^* received from the layer below (whilst this lower layer is maintained) and additionally from the jet-like inflow, Q_j. The reduced gravity of the jet is zero, and thus it does not contribute to the flux of buoyancy supplied to the middle layer. Volume- and buoyancy-flux conservation for the middle layer require, respectively

$$S\frac{\mathrm{d}}{\mathrm{d}t}(h_u - h_l) = Q^* + Q_j \quad \text{and} \quad S\frac{\mathrm{d}}{\mathrm{d}t}[g'_m(h_u - h_l)] = Q^* g'_l. \tag{2.1b}$$

To close the problem, three fluxes are required: Q, Q_j and Q^*.

2.1.1. *Volume flux through the box (Q)*

This flux is a function of the top and base opening areas, and the total buoyancy $\mathcal{B} = S \int_0^H g'(z, t)\,\mathrm{d}z$ within the box:

$$Q = A^* \left(\frac{\mathcal{B}}{S}\right)^{1/2}, \quad A^* = \left(\frac{1}{2c_B^2 a_B^2} + \frac{1}{2c_T^2 a_T^2}\right)^{-1/2}, \tag{2.2}$$

where A^* is the 'effective opening area', see Linden *et al.* (1990).

2.1.2. *Volume flux in the jet-like inflow (Q_j)*

Assuming that the inflow behaves as a fully developed self-similar turbulent jet, from classic jet scalings (Fischer *et al.* 1979), the centreline vertical velocity, jet width and volume flux at the level of the upper interface are

$$w_j = 7.0 M_T^{1/2} L^{-1}, \quad b_j = 0.107L \quad \text{and} \quad Q_j = 0.25 M_T^{1/2} L, \tag{2.3}$$

respectively, where $L = H - h_u + z_v$ is the distance between the virtual origin of the jet (a distance z_v above the top opening) and the upper interface. In (2.3), M_T denotes the momentum flux through the top opening at $z = H$, i.e. the source momentum flux of the jet. Assuming the velocity profile across the opening is uniform, a reasonable assumption for high Reynolds number flow, $M_T = Q^2/a_T$. We have used a geometric origin correction based on tracing the jet perimeter back to a point, thus setting $b_j(z = H) = \sqrt{a_T/\pi}$ in (2.3), $z_v = \sqrt{a_T/\pi}/0.107$.

2.1.3. *Volume flux entrained across the density interface (Q^*)*

We consider the formulations for entrainment fluxes across density interfaces developed by Baines (1975), Kumagai (1984) and Lin & Linden (2005). Baines (1975) performed experiments investigating the entrainment due to turbulent plumes and jets impinging on density interfaces. By tracking the position of the interface, he inferred the volume flux turbulently entrained across it. Baines's results agree with the scalings of previous investigations (e.g. Linden 1973) with the entrainment flux being proportional to the cube of a Froude number. Examination of the experimental data (figure 2 in Baines 1975, and figure 3 herein) suggests

$$\text{I.} \quad \frac{Q^*}{b_l^2 w_l} = 0.67 Fr_T{}^3, \quad Fr_T = \frac{w_l}{\sqrt{b_l \Delta g'}}, \tag{2.4a}$$

where b_l and w_l are the jet/plume width and centreline vertical velocity at the interface, respectively. The width and velocity may be inferred from (2.3). The buoyancy step across the interface is denoted $\Delta g' = g_l' - g_m'$. Baines (1975) assumed Gaussian profiles for the velocity of the impinging flow, so we have rescaled his data, using $Fr_{T\,tophat} = 2^{-5/4} Fr_{T\,Gaussian}$ (as $w_{tophat} = 2^{-1} w_{Gaussian}$ and $b_{tophat} = 2^{1/2} b_{Gaussian}$) to infer the constant of proportionality 0.67. The interfacial Froude numbers are estimated in our model using the characteristic vertical velocity and width scales of a turbulent jet. For $t > 0$, the inflow must penetrate a layer of fluid with reduced gravity g_m' (>0) and, as a consequence, the impinging flow develops as a fountain in the middle layer. Kaye & Hunt (2006) demonstrate for a wide range of fountain source Froude numbers Fr_f that the flow in a fountain is jet-like over the vast majority of the rise height and hence, the jet scalings adopted are expected to be appropriate.

Kumagai (1984) performed a series of experiments similar to those of Baines (1975). Kumagai's data suggest that the entrainment flux obeys the $Fr_T{}^3$ law for small Froude numbers but tends to a constant value (of 0.56) for larger Froude numbers

$$\text{II.} \qquad \frac{Q^*}{b_l^2 w_l} = \frac{1.0 Fr_T{}^3}{1 + 3.1 Fr_T{}^2 + 1.8 Fr_T{}^3}. \qquad (2.4b)$$

Lin & Linden (2005) also investigated entrainment across density interfaces due to the impingement of jets and plumes. For $0.9 \leqslant Fr_T \leqslant 2.2$, i.e. towards the higher end of Fr_T generally considered, the entrainment flux was approximately constant with

$$\text{III.} \qquad \frac{Q^*}{b_l^2 w_l} \approx 2.0. \qquad (2.4c)$$

This flux is over four times greater than that expected from the empirical formulation of Kumagai (1984) for large Fr_T. The result that $Q^* \propto b_l^2 w_l$ suggests that the stability of the interface, i.e. the buoyancy step $\Delta g'$, has no bearing on the rate of entrainment across it even at relatively low Froude numbers (e.g. $Fr_T \approx 0.9$).

To allow comparison, figure 3 plots Fr_T against $Q^*/(b_l^2 w_l)$ for each formulation, together with the respective authors' data. A significant amount of scatter is evident in the data although the reasons for this are not entirely clear. However, estimating the interfacial Froude numbers accurately for these experiments is difficult as, for example, plume width b_l and vertical velocity w_l on impingement were not measured directly but based on estimates from plume theory with a suitable origin correction. Moreover, the entrainment fluxes were also not measured directly but inferred from measurements of front movement. We shall evaluate our model for the emptying of the box using each of the formulations (2.4a), (2.4b) and (2.4c) which hereafter we refer to as mixing models I, II and III, respectively.

Observations and predictions indicate that turbulent entrainment is most vigorous during the early stages of a purge. At later times, observations show that the impingement of the fountain with the original-layer/middle-layer interface may cease (Hunt & Coffey 2010, figure 6) and the fountain-top entrainment flux from the lower layer thereby reduces to zero. We invoke a simplified model for the development of the inflow through the middle layer, namely, that of a highly forced fountain, and do not capture the aforementioned effect. Figure 4 plots the predicted decrease of Fr_T with time indicating a reduction in entrainment flux (see (2.4a) or (2.4b)). In principle, our model could be adapted in order to 'switch' entrainment off once the fountain fails to reach the interface, in other words when the middle layer depth ($h_u - h_l$) exceeds the fountain's rise height. The behaviour of the fountain in the middle layer
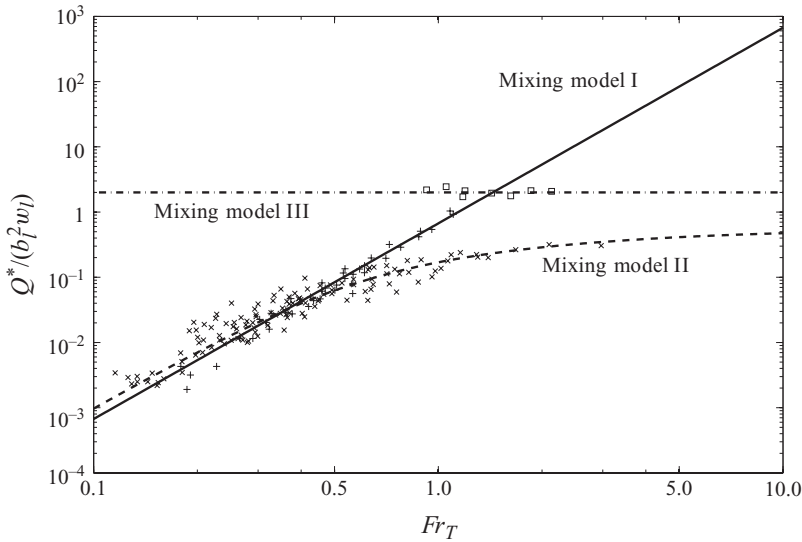
FIGURE 3. Fr_T against $Q^*/(b_l^2 w_l)$ for each of the mixing formulations considered. The solid line shows model I, the dashed line shows model II and the dashed-dotted line shows model III. Also shown is the experimental data of Baines (1975) ($+$), Kumagai (1984) ($\times$) and Lin & Linden (2005) ($\square$).
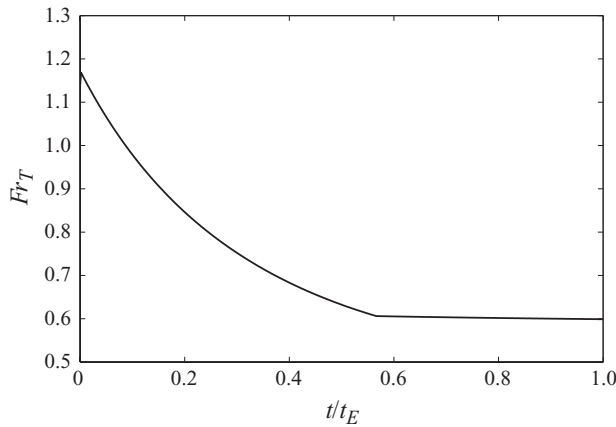

FIGURE 4. The typical variation of Fr_T with dimensionless time based on mixing model II for which the entrainment flux is defined in (2.4b). The change in gradient for $t/t_E \gtrsim 0.55$ corresponds to the removal of the original lower layer. Thereafter, there is a slow decrease in Fr_T.

is complex and the scaling for its penetration depth varies with Fr_f. Kaye & Hunt (2006) show that there are multiple fountain regimes each with a different rise height dependence on Fr_f. Moreover, the fountain source conditions are time-varying and the environment is not quiescent. Including this extra layer of complexity to the model is unlikely to lead to further physical insight and the close agreement achieved on comparison with measurements (§ 3) shows that the potential overestimation of entrainment flux for large times does not have a marked effect.

2.2. Non-dimensionalization

Dimensionless (hatted) variables are now introduced as follows:

$$\hat{t} = \frac{t}{t_E}, \quad \hat{Q} = \frac{Q}{Q_0}, \quad \hat{h} = \frac{h}{h_0}, \quad \hat{g}' = \frac{g'}{g_0'}, \quad \hat{b} = \frac{b}{\sqrt{A^*}}, \quad \hat{w} = \frac{w}{(h_0 g_0')^{1/2}}. \tag{2.5}$$

The time scale $t_E = (2S/A^*)(h_0/g_0')^{1/2}$ is the time taken to empty (i.e. drain out of the box) a dense fluid layer of initial depth h_0 in the absence of mixing (see Linden *et al.* 1990), $Q_0 = A^*(h_0 g_0')^{1/2}$ is the volume flux through the box at $t=0$ (see (2.2)), and $(h_0 g_0')^{1/2}$ is a characteristic buoyancy-induced velocity with characteristic reduced gravity identical to that of the initial lower layer, i.e. $g_0' = g_l'(t=0)$. The jet width is scaled on $\sqrt{A^*}$ as this provides a characteristic opening radius through which the jet propagates and allows the governing equations to be reduced to their simplest form. On substituting for R, ξ_0 and λ_T from (1.1) and non-dimensionalizing, the governing equations (2.1) reduce to

$$\frac{1}{2}\frac{d\hat{h}_l}{d\hat{t}} = -(\hat{Q}+\hat{Q}^*), \quad \frac{1}{2}\frac{d}{d\hat{t}}(\hat{h}_u - \hat{h}_l) = \hat{Q}^* + \hat{Q}_j \quad \text{and} \quad \frac{1}{2}\frac{d}{d\hat{t}}[\hat{g}_m'(\hat{h}_u - \hat{h}_l)] = \hat{Q}^*. \tag{2.6a}$$

The dimensionless volume flux through the box, $\hat{Q}$, in the inflowing jet, $\hat{Q}_j$, and turbulently entrained $\hat{Q}^*$ are, from (2.2), (2.3) and (2.4), respectively

$$\hat{Q} = [\hat{h}_l + \hat{g}_m'(\hat{h}_u - \hat{h}_l)]^{1/2}, \quad \hat{Q}_j = 0.25\hat{Q}\frac{1}{\lambda_T}\left(\frac{1}{\xi_0} - \hat{h}_u + \hat{z}_v\right), \tag{2.6b}$$

and

$$\text{I.} \quad \frac{\hat{Q}^*}{\hat{b}_l^2 \hat{w}_l} = 0.67 Fr_T{}^3, \quad \text{II.} \quad \frac{\hat{Q}^*}{\hat{b}_l^2 \hat{w}_l} = \frac{1.0 Fr_T{}^3}{1 + 3.1 Fr_T{}^2 + 1.8 Fr_T{}^3} \quad \text{or} \quad \text{III.} \quad \frac{\hat{Q}^*}{\hat{b}_l^2 \hat{w}_l} = 2.0, \tag{2.6c}$$

where

$$Fr_T = 2^{-1/8}\frac{R^{*1/4}}{\lambda_T^{1/2}}\frac{\hat{w}_l}{(\hat{b}_l(1 - \hat{g}_m'))^{1/2}}, \tag{2.6d}$$

$$\hat{w}_l = 7\sqrt{2}\frac{\lambda_T}{R^*}\left(\frac{1}{\xi_0} - \hat{h}_l + \hat{z}_v\right)^{-1}, \quad \hat{b}_l = 0.107 \times 2^{-1/4}\frac{R^{*1/2}}{\lambda_T}\left(\frac{1}{\xi_0} - \hat{h}_l + \hat{z}_v\right), \tag{2.6e}$$

$$R^* = \left(\frac{1}{c_T^2} + R^2\frac{1}{c_B^2}\right)^{1/2} \quad \text{and} \quad \hat{z}_v = \frac{\lambda_T}{0.107\pi^{1/2}}. \tag{2.6f}$$

The system of equations (2.6a)–(2.6f) were solved using Runge–Kutta methods of orders four and five for a given point in the $\{R, \lambda_T, \xi_0\}$ parameter space subject to the initial conditions

$$\hat{h}_l(\hat{t}=0) = 1, \quad \hat{g}_u'(\hat{t}=0) = 0, \quad \hat{h}_u(\hat{t}=0) = 1, \quad \hat{g}_m'(\hat{t}=0) = 0, \quad \hat{g}_l'(\hat{t}=0) = 1. \tag{2.7}$$

The middle layer has zero thickness at $\hat{t}=0$ and, hence, for any finite $\hat{g}_m'(\hat{t}=0)$, the total buoyancy contained in this layer is initially zero. As a consequence, the layer does not contribute at $\hat{t}=0$ to driving the flow. Furthermore, as no mixing has occurred at $\hat{t}=0$, and thus no buoyant fluid has been drawn into the middle layer we have chosen $\hat{g}_m'(\hat{t}=0) = 0$.

No.	Symbol	R	λ_T	ξ_0	A^* (cm^2)	g_0' (cm s^{-2})	t_E (s)	$Fr_T(0)$
1	☆	13.0	1.28	0.41	16.1	37.2	85.6	0.08
2	+	3.80	0.57	0.50	16.1	15.7	146.3	0.33
3	▽	0.36	0.36	0.24	5.4	37.2	196.8	0.54
4	×	0.22	0.14	0.50	3.6	18.8	597.6	1.08
5	✿	0.21	0.13	0.51	3.4	18.7	638.9	1.09
6	*	0.36	0.17	0.52	5.7	13.3	461.1	1.18
7	○	0.36	0.16	0.53	5.2	35.6	310.4	1.20
8	□	1.0	0.23	0.63	11.3	35.6	154.2	1.22
9	△	0.36	0.15	0.6	5.8	45.1	260.5	1.46
10	◇	0.36	0.13	0.70	6.0	37.2	303.0	1.89
Experiment 1	◁	5.66	0.22	1.0	4.3	–	–	0.39
Experiment 2	▷	2.28	0.29	1.0	18.4	–	–	0.87

TABLE 1. Conditions for the experiments (numbered 1–10) presented in §3. For the experiments we performed, $S = 1200$ cm^2 and $H = 30$ cm. We have taken $c_T = c_B = 0.6$ (Ward-Smith 1980) to estimate A^* and t_E. Experiments 1 and 2 refer to the experiments of Linden *et al.* (1990).

3. Model validation

A series of experiments were performed, where R, λ_T and ξ_0 were varied such that $Fr_T(0)$ increased (see table 1), using the same emptying-box rig described by Hunt & Coffey (2010). Density profiles were deduced using a dye-attenuation technique (Cenedese & Dalziel 1998; Hunt & Coffey 2010). The heights of the interfaces between layers were then determined by locating peaks in the gradient of the density profiles. Data from Linden *et al.* (1990), experiments 1 and 2 in table 1, were also compared with our model.

Figure 5 plots the dimensionless depth of the lower layer ($\hat{h}_l = h_l/h_0$) against dimensionless time ($\hat{t} = t/t_E$) for each of our 10 experimental runs. Theoretical predictions are plotted for each of the formulations of Q^* (I, II and III; see (2.4)).

Predictions based on mixing models I and II both provide good agreement with the experimental results for low values of $Fr_T(\ll 0.67)$ where interfacial mixing was not observed in experiments (e.g. for runs 1 and 2, the predictions based on I and II differ by less than 1 % and are graphically indistinguishable in our plots). For both I and II, $Q^*/(b_l^2 w_l) \sim Fr_T^3 \ll 1$ for $Fr_T \ll 1$, hence, the predicted interfacial mixing is negligible and in this limit the two models are equivalent. As Fr_T is increased, mixing model I over predicts the volume flux of fluid turbulently entrained from the lower layer; apparent by the lower interface descending too rapidly compared with measurements (see runs 7–10). Conversely, mixing model II under predicts the entrainment flux; apparent by the lower interface descending too slowly compared with measurements. Mixing model III provides the best comparison at large Froude numbers.

Figure 6(*a*) shows a time series of the horizontally averaged dimensionless reduced gravity profiles in the box, measured using the dye-attenuation technique, and figure 6(*b*) a time series of the corresponding theoretical predictions. Figure 6(*c*) shows the difference between the experimental results and the theoretical predictions. Mixing model II yields the most reliable predictions to the overall developing density stratification. The predictions based on mixing models I and III are poorer, with an over prediction of the reduced gravity in the middle layer (evident by the red-coloured region in figure 6*c*).
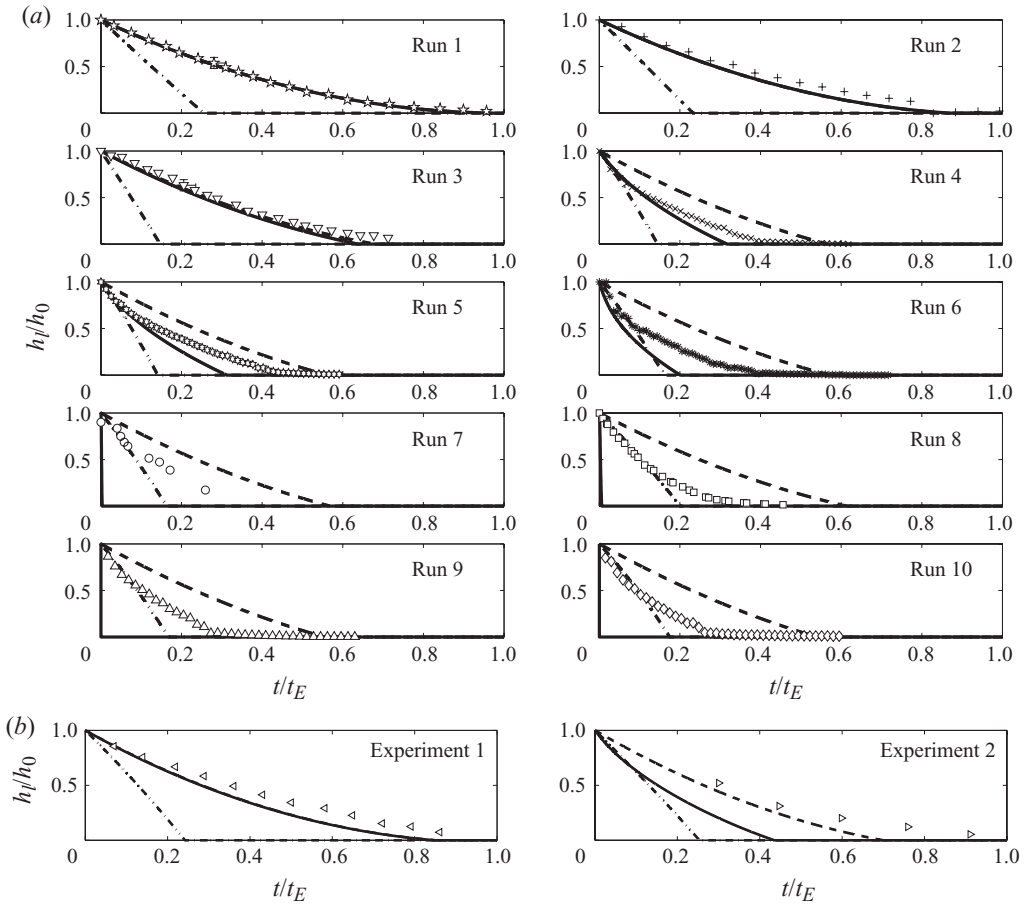
FIGURE 5. Lower interface height h_l/h_0 versus time t/t_E. Predictions show: mixing models I (solid line), II (dashed line) and III (dashed-dotted line). Error bars typical for all runs are shown on a single data point in runs 1 and 3. The value of $Fr_T(0)$, and thus the expected/observed vigour of interfacial mixing, increases from runs 1–10 (see table 1). (*a*) The present experiments. (*b*) Experiments by Linden *et al.* (1990).

The time series highlight a limitation of the model. Though two distinct density interfaces are evident (regions of rapidly changing colour in figure 6*a*), the middle layer is not uniform in the early transients. This is most apparent in the contouring visible in the middle layer of figure 6(*c*), which shows the difference between theory and experiment for run 5. However, the theoretical model developed (particularly when mixing model II is used) predicts the broad characteristics of the developing stratification remarkably well for a simplified model.

4. Analytical solutions

The governing equations (2.6) may be solved analytically for two cases, namely for mixing model I under the assumption that $\hat{g}'_m \ll 1$ (i.e. $\Delta g' \approx g'_l$), and directly for mixing model III.

Whilst a lower layer of the original density ρ_0 remains, i.e. for $h_l > 0$, the volume flux Q is dependent solely on the total box-integrated buoyancy $\mathscr{B}$ (see §2.1.1, (2.2))
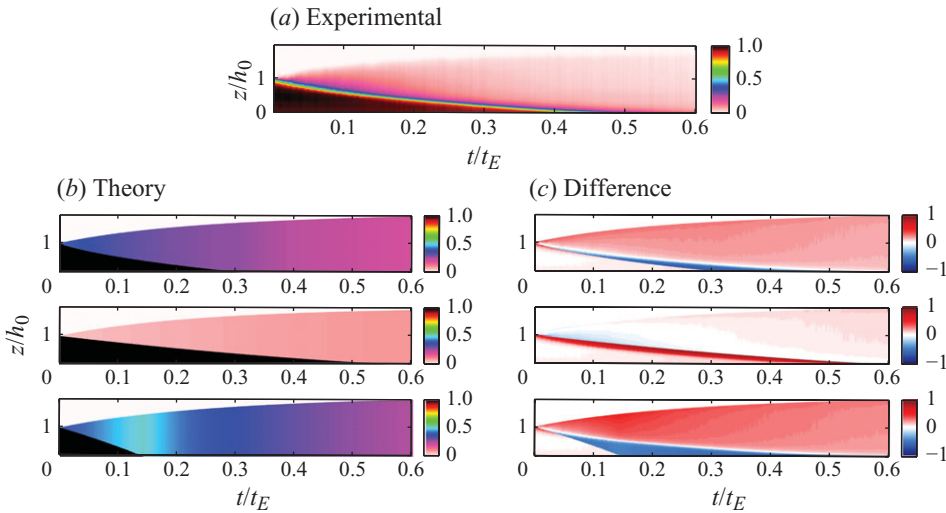
FIGURE 6. Time series of the non-dimensionalized reduced gravity $\hat{g}' = g'/g_0'$ profile within the box. The colour at a given point denotes $\hat{g}'$ at the corresponding depth $\hat{z} = z/h_0$ and time $\hat{t} = t/t_E$. (a) As measured in experiment (run 5) and (b) as predicted with mixing models I, II and III (from top to bottom). (c) Difference between experimental results (a) and theoretical predictions (b). The positions of the upper and lower interfaces can be clearly seen.

and is independent of the buoyancy distribution. In other words, at this stage, the interfacial mixing that has occurred has no influence on the rate of draining Q. Thus, the dimensionless volume flux may be written explicitly in terms of $\hat{t}$ as

$$\hat{Q} = 1 - \hat{t} \quad \text{for} \quad \hat{h}_l > 0. \tag{4.1}$$

4.1. Case 1. Mixing model I, $\hat{g}'_m \ll 1$

The flux entrained from lower to middle layer is, from (2.4a) and (2.6d),

$$\hat{Q}^* = 0.67\hat{b}_l^2 \hat{w}_l Fr_T{}^3 = d_1 \frac{\lambda_T^2}{R^{*3}} \left(\frac{1}{\xi_0} - \hat{h}_l + \hat{z}_v \right)^{-7/2} (1 - \hat{g}'_m)^{-3/2}, \tag{4.2}$$

where $d_1 = 0.67 \times 0.107^{1/2} \times 7^4 \times 2^{3/2}$. Assuming $\hat{g}'_m \ll 1$, (4.2) reduces to

$$\hat{Q}^* = d_1 \frac{\lambda_T^2}{R^{*3}} \left(\frac{1}{\xi_0} - \hat{h}_l + \hat{z}_v \right)^{-7/2}. \tag{4.3}$$

The source momentum flux and Reynolds number for the inflowing jet are dependent on the instantaneous volume flux ($\propto \mathscr{B}(t)^{1/2}$, (2.2)) and the area of the vent through which the jet issues. As $\mathscr{B}(t)$ is a decreasing function of time, after some period the Reynolds number for the flow through the openings will be sufficiently low that viscous effects begin to play a role in the subsequent draining – this low-Reynolds-number regime is not considered herein. Thus, the condition $\hat{g}'_m \ll 1$ is not incompatible with having turbulent jets at the inlet and outlet other than for sufficiently large times when little total buoyancy $\mathscr{B}(t)$ remains in the box. From (2.6a), conservation of volume requires

$$\frac{1}{2} \frac{\mathrm{d}\hat{h}_l}{\mathrm{d}\hat{t}} = -(\hat{Q} + \hat{Q}^*) = -1 + \hat{t} - d_1 \frac{\lambda_T^2}{R^{*3}} \left(\frac{1}{\xi_0} - \hat{h}_l + \hat{z}_v \right)^{-7/2}. \tag{4.4}$$

Substituting $\omega = d_1(\lambda_T^2/R^{*3})$ and $\chi = ((1/\xi_0) - \hat{h}_l + \hat{z}_v)$ yields

$$\frac{1}{2}\frac{d\chi}{d\hat{t}} = 1 - \hat{t} + \omega\chi^{-7/2}, \tag{4.5}$$

where χ is the dimensionless distance between the virtual origin of the inflowing jet and the lower interface position. Denoting $\chi_0 \equiv \chi(\hat{t}=0) = ((1/\xi_0) - 1 + \hat{z}_v)$, solving (4.5) gives

$$\chi(\hat{t}) = \chi_0 + 2\frac{\chi_0^{7/2} + \omega}{\chi_0^{7/2}}\hat{t} - \frac{\chi_0^8 + 7\omega\chi_0^{7/2} + 7\omega^2}{\chi_0^8}\hat{t}^2$$
$$+ \frac{7}{3}\frac{\omega\left(\chi_0^8 + 25\omega\chi_0^{7/2} + 16\omega^2 + 9\chi_0^7\right)}{\chi_0^{25/2}}\hat{t}^3 + O(\hat{t}^4). \tag{4.6}$$

4.2. Case 2. Mixing model III

From (2.4c),

$$\hat{Q}^* = 2.0\hat{b}_l^2\hat{w}_l = d_2\frac{1}{\lambda_T}\left(\frac{1}{\xi_0} - \hat{h}_l + \hat{z}_v\right), \tag{4.7}$$

where $d_2 = 7 \times 2.0 \times 0.107^2$. Conservation of volume for the lower layer (2.6a) requires

$$\frac{1}{2}\frac{d\chi}{d\hat{t}} = 1 - \hat{t} + \psi\chi, \tag{4.8}$$

where $\psi = d_2/\lambda_T$, which may be solved directly to give

$$\chi(\hat{t}) = \frac{1}{2\psi^2} + \frac{1}{\psi}(\hat{t}-1) + e^{2\psi\hat{t}}\left(\chi_0 + \frac{1}{\psi} - \frac{1}{2\psi^2}\right). \tag{4.9}$$

Figure 7 plots the experimental data and interface positions predicted by solutions (4.6) and (4.9). The series solution (4.6) provides a very good match to the experimental data. It is noteworthy that the two-layer model proposed by Linden et al. (1990) extended with additional terms to account for the entrainment flux, the final term in (4.5) and (4.8) shows such good agreement with the measurement.

5. Discussion

Further examination of the theoretical model developed enables additional insight into unidirectional emptying-box flows. By comparing the predictions and the experimental data for the three mixing models, and by applying the model to a wider range of parameter space than can be effectively or reasonably investigated in the laboratory, we are able to comment on entrainment fluxes across density interfaces and draining times.

5.1. Entrainment across density interfaces

The developing stratification in the emptying boxes examined was well predicted by mixing models I and II for small Fr_T, and by mixing model III for large Fr_T (figure 5). These results support the findings of Kumagai (1984), i.e. that the non-dimensional entrainment flux scales as the cube of Fr_T for small Fr_T and tends to a constant value for large Fr_T. Runs 9 and 10 indicate that this constant value lies between that suggested by Kumagai (1984) and by Lin & Linden (2005), i.e.

$$\left.\begin{array}{ll} 0.56 \lesssim Q^*/b_l^2 w_l \lesssim 2.0 & \text{for} \quad Fr_T \gg 1, \\ Q^*/b_l^2 w_l \propto Fr_T^3 & \text{for} \quad Fr_T \ll 1. \end{array}\right\} \tag{5.1}$$
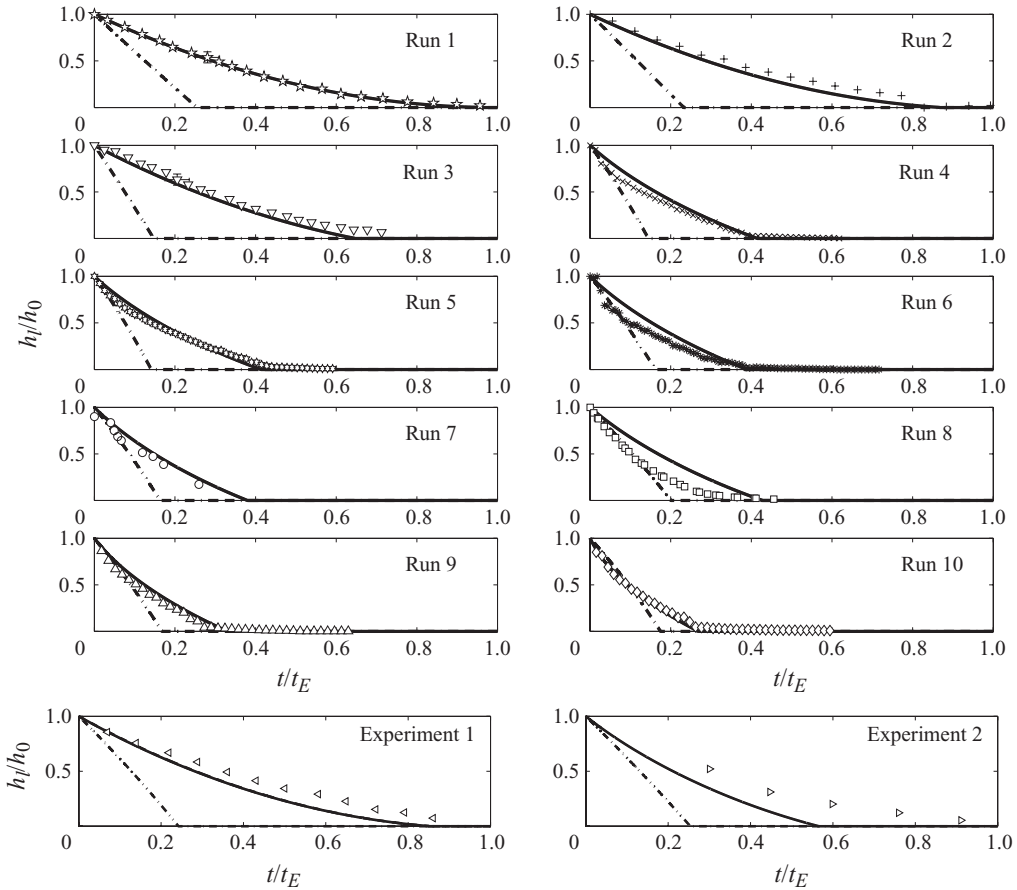
FIGURE 7. Dimensionless interface height versus dimensionless time. The solid line is the series solution (4.6) and the dashed-dotted line the analytical solution (4.9).

5.2. *Draining times*

Given, for a range of initial conditions, the original layer will have drained completely from the box after some time, t_D say, leaving a two-layer system (i.e. a mixed layer below a layer at ambient density) and, thereby, a basic stratification not dissimilar from that at $t = 0$, the question of whether the flow is cyclic arises. This is not the case, however as unlike the dynamics initiated from $t = 0$, in which the inflowing jet is confined within the middle layer and notably does not penetrate through the lower layer (whose density remains constant), for $t > t_D$ inflow penetrates the mixed layer which gradually dilutes with time.

In contrast to the classical displacement flows described by Linden *et al.* (1990), the unidirectional emptying box does not generally drain completely (i.e. empty) of buoyant fluid in a time t_E. However, we may define a draining time t_D as the time taken for the lower interface to reach the base of the box so that at $t = t_D$, all fluid of the lower layer density at $t = 0$ has emptied from the box. As fluid is only ever removed from the lower layer, t_D is bounded from above by the classical displacement flow emptying time, i.e. $t_D \leqslant t_E$. From (5.1), the non-dimensional entrainment volume

flux is bounded by

$$0 \leqslant \frac{\hat{Q}^*}{\hat{b}_l^2 \hat{w}_l} \leqslant \text{const.}$$

with the models of Kumagai (1984) and Lin & Linden (2005) suggesting this constant is in the range 0.56–2.0. The lower bound $\hat{Q}^*/\hat{b}_l^2 \hat{w}_l = 0$ being that entrained when $Fr_T = 0$. Thus, from (2.6a),

$$-\hat{Q} \leqslant \frac{1}{2} \frac{\mathrm{d}\hat{h}_l}{\mathrm{d}\hat{t}} = -(\hat{Q} + \hat{Q}^*) \leqslant -(\hat{Q} + 2.0\hat{b}_l^2 \hat{w}_l). \tag{5.2}$$

This may be solved to give

$$2\hat{t} - \hat{t}^2 + \chi_0 \leqslant \chi \leqslant \frac{1}{2\psi^2} + \frac{1}{\psi}(\hat{t} - 1) + e^{2\psi\hat{t}}\left(\chi_0 + \frac{1}{\psi} - \frac{1}{2\psi^2}\right). \tag{5.3}$$

Thus, the non-dimensional draining time $\hat{t}_D = t_D/t_E$ is bounded by

$$a \geqslant \hat{t}_D \geqslant b, \tag{5.4}$$

where

$$a = 1, b = \frac{1}{2\psi}\left[-1 + 2\psi + 2\psi^2 + 2\psi^2\chi_0 - W\left(e^{-1+2\psi+2\psi^2+2\psi^2\chi_0} \times [-1 + 2\psi + 2\psi^2\chi_0]\right)\right], \tag{5.5}$$

and $W(x)$ is the Lambert W-function. (5.4) indicates that the lower bound on $\hat{t}_D$ is a function of ψ ($\propto 1/\lambda_T$) and χ_0 (a function of ξ_0 and λ_T), and is independent of R. Figure 8 shows contours of the lower bound on $\hat{t}_D$ in the $\{\lambda_T, \xi_0\}$ parameter space. Decreasing λ_T or ξ_0 results in a decrease in this lower bound. Whilst for sufficiently small λ_T or ξ_0 we are able to reduce this lower bound to zero, the contours indicate that for a significant portion of the parameter space $\hat{t}_D > 0.2$.

Figure 9 shows t_D for various slices through the $\{R, \lambda_T, \xi_0\}$ parameter space calculated through successive runs of the theoretical model using mixing model II. These explorations of the parameter space also suggest that $\hat{t}_D$ is bounded from below and, thus, that the lower layer can not be removed faster than some proportion of t_E.

6. Implications for night cooling

To highlight some implications of interfacial mixing to a night-cooling application, we consider the purging of a room the size of a typical open plan office. The opening area is taken as 1 % of the 225 m^2 floor area (a percentage in keeping with accepted design guidance, Etheridge & Sandberg 1984). The purge is initiated by a layer that is initially two-thirds of the floor to ceiling height of 3 m and 15°C warmer than the exterior night air at 5°C.

In figure 10, we plot four cases, focusing on the dimensionless warm-layer depth variation with time and mean interior–exterior temperature difference for the initial conditions given in table 2. These cases illustrate the sensitivity of night purging to
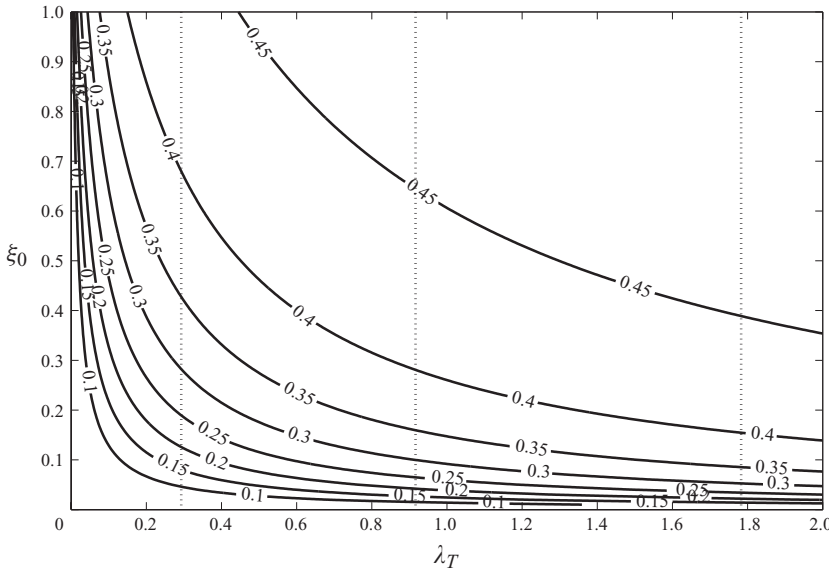
FIGURE 8. Contours of the draining time lower bound from (5.4). From left to right each vertical line corresponds to $Fr_B = 0.33$ at the values $R = 0.3$, 0.5 and 0.7. As unidirectional flow requires $Fr_B \gtrsim 0.33$ (figure 2), the bound on $\hat{t}_D$ for a given R is only valid to the left of the corresponding vertical line.

the distribution of the ventilation openings. In figure 10,

$$\frac{\overline{\Delta T(t)}}{\overline{\Delta T_0}} = \frac{\int_0^H \Delta T(z, t)\,\mathrm{d}z}{\int_0^H \Delta T_0(z)\,\mathrm{d}z}, \qquad (6.1)$$

where $\Delta T(z, t)$ is the temperature difference between the interior and exterior at a height z and time t, and $\Delta T_0(z) = \Delta T(z, t = 0)$. It is clear that the rate of purging of warm air from the layer (figure 10a) may be significantly enhanced, without the need for increasing the total opening area, by simply reducing the area of the lower vent relative to the upper. Additionally, figure 10(b) shows that the normalized temperature difference increases over the time interval shown on reducing the area of the lower vent relative to the upper. An architect, or designer, may therefore control a night purge by adjusting the relative areas of the vents.

7. Conclusions

Hunt & Coffey (2010) showed that the emptying of dense fluid from a box that connects to an external environment through high and low-level openings may lead to a layered internal stratification and that the stratification can be well approximated by three well-mixed layers.

Under this assumption, we have developed a model to predict the evolving stratification. Focusing on the portion of the parameter space where unidirectional flows occur through both top and base openings ($Fr_B(0) > 0.33$, Hunt & Coffey 2010), we have shown through the use of simple modelling techniques that good predictions of the developing stratification are possible.
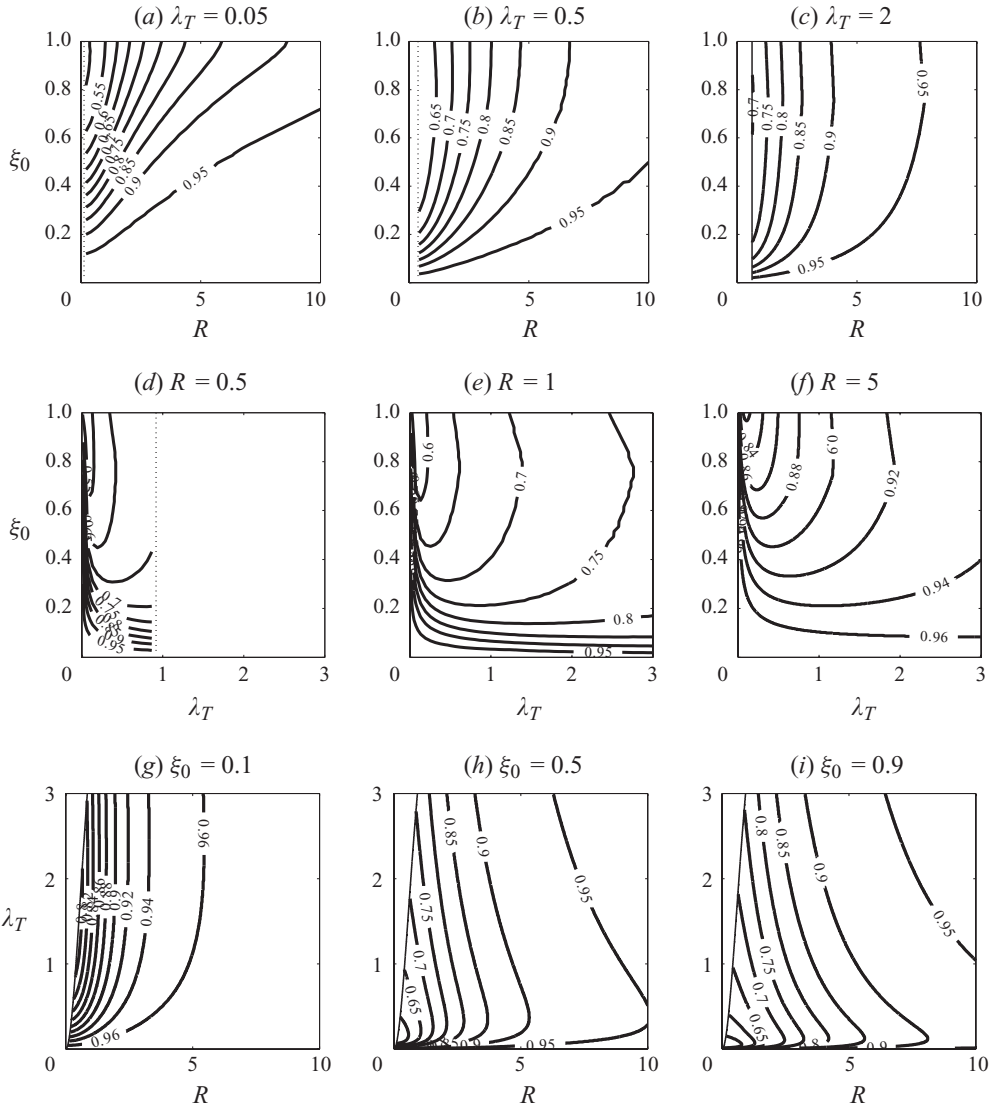
FIGURE 9. Dimensionless time $\hat{t}_D$ taken to remove the original lower layer, i.e. $\hat{t}_D$ for which $\hat{h}_l(\hat{t} = \hat{t}_D) = 0$. Contours of constant $\hat{t}_D$ are shown for various slices through the $\{R, \lambda_T, \xi_0\}$ parameter space. The effect of the initial layer depth is depicted in (a)–(f). The effect of the box geometry is depicted in (g)–(i). Contours are drawn only for the region of parameter space where unidirectional flow is expected (i.e. for $Fr_B(0) \gtrsim 0.33$, denoted by the dotted line).

The model has allowed three different formulations describing the mixing across density interfaces developed previously by Baines (1975), Kumagai (1984) and Lin & Linden (2005) to be compared in this application. These models were shown to vary in their ability to predict the interfacial mixing over different regions of the parameter space. The experiments presented herein support the hypothesis that for small Froude numbers (Fr_T) the normalized volume flux ($Q^*/(b_l^2 w_l)$) turbulently entrained across an interface scales like the cube of the Froude number. Conversely, for large Froude numbers the normalized entrainment flux tends to a constant value (0.56–2.0). Due

Case	Upper opening (%)	Lower opening (%)	R	λ	ξ_0	Fr_T	Fr_B
1	20	80	4	0.67	0.67	0.37	1.42
2	40	60	1.5	0.58	0.67	0.87	1.03
3	50	50	1	0.53	0.67	1.14	0.82
4	60	40	0.67	0.47	0.67	1.38	0.62

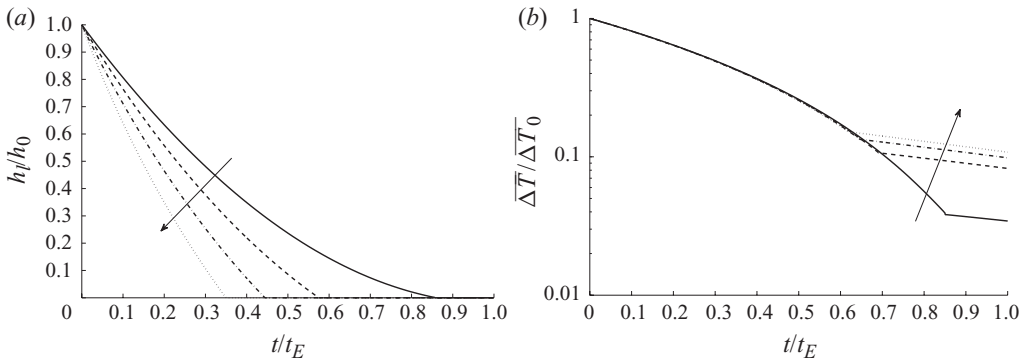TABLE 2. Room opening distribution, geometric ratios and vent Froude numbers.

FIGURE 10. Plots of normalized (*a*) warm-layer depth and (*b*) mean temperature difference between interior and exterior against time based on model II. Arrows indicate predictions for decreasing upper opening area (i.e. case 1 through to case 4) for the conditions given in table 2.

to the large amount of scatter present in measurements of entrainment fluxes (see figure 3), one might argue that a simple formulation for the entrainment flux is as appropriate as the more complicated relationship suggested by Kumagai (1984), (2.4*b*). For example, one might expect the entrainment flux to follow

$$\frac{Q^*}{b_l^2 w_l} \propto \left(1 + \frac{1}{Fr_T{}^3}\right)^{-1}.$$

The upper bound on the entrainment flux (achieved as $Fr_T \to \infty$) implies that it is not possible to remove the lower layer faster than some minimum time. By considering the limiting cases of the model (i.e. minimizing and maximizing the entrainment flux), we have shown that the time to remove the lower layer t_D is bounded by $t_E \geqslant t_D \gtrsim 0.2 t_E$. This has implications when considering, for example, flushing of heat from a room. One approach may be to deliberately mix the air as the warmer interior air is purged in order to create a reasonably well-mixed interior of a (comfortable) temperature between that of the cool exterior and the temperature at the beginning of the purge. Our analysis suggests that, for a given A^*, there is a minimum time required to mix the interior and that this time exceeds approximately 1/5 of the classical emptying time t_E.

REFERENCES

BAINES, W. D. 1975 Entrainment by a plume or jet at a density interface. *J. Fluid Mech.* **68** (2), 309–320.

BAINES, W. D. & TURNER, J. S. 1969 Turbulent buoyant convection from a source in a confined region. *J. Fluid Mech.* **37**, 51–80.

CARDOSO, S. S. S. & WOODS, A. W. 1993 Mixing by a turbulent plume in a confined stratified region. *J. Fluid Mech.* **250**, 277–305.

CENEDESE, C. & DALZIEL, S. B. 1998 Concentration and depth field determined by the light transmitted through a dyed solution. In *Proceedings of the Eighth International Symposium on Flow Visualization*, Sorrento, Italy.

COFFEY, C. J. & HUNT, G. R. 2007 Ventilation effectiveness measures based on heat removal. Part 1. Definitions. *Build. Environ.* **42** (6), 2241–2248.

ETHERIDGE, D. W. & SANDBERG, M. 1984 A simple parametric study of ventilation. *Build. Environ.* **19** (3), 163–173.

FERNANDO, J. & SMITH, D. C. 2001 Vortex structures in geophysical convection. *Eur. J. Mech.* B – *Fluids* **20**, 437–470.

FISCHER, H. B., LIST, E. J., KOH, R. C. Y., IMBERGER, J. & BROOKS, N. H. 1979 *Mixing in Inland and Coastal Waters*. Academic Press, ISBN 0-12-258150-4.

HUNT, G. R. & COFFEY, C. J. 2010 Emptying boxes – classifying transient natural ventilation flows. *J. Fluid Mech.* **646**, 137–168.

KAYE, N. B. & HUNT, G. R. 2006 Weak fountains. *J. Fluid Mech.* **558**, 319–328.

KUMAGAI, M. 1984 Turbulent buoyant convection from a source in a confined two-layered region. *J. Fluid Mech.* **147**, 105–131.

LIN, Y. J. P. & LINDEN, P. F. 2005 A model for an under floor air distribution system. *Energy Build.* **37** (4), 399–409.

LINDEN, P. F. 1973 The interaction of a vortex ring with a sharp density interface: a model for turbulent entrainment. *J. Fluid Mech.* **60**, 467–480.

LINDEN, P. F. 1999 The fluid mechanics of natural ventilation. *Annu. Rev. Fluid Mech.* **31**, 201–238.

LINDEN, P. F., LANE-SERFF, G. F. & SMEED, D. A. 1990 Emptying filling boxes, the fluid mechanics of natural ventilation. *J. Fluid Mech.* **212**, 309–335.

PARK, O. H., SEO, S. J. & LEE, S. H. 2001 Laboratory simulation of vertical plume dispersion within a convective boundary layer. *Bound.-Layer Meteorol.* **99**, 159–169.

PRESLEY, J. D. & TELFORD, J. W. 1988 Turbulent entrainment at an inversion. *J. Pure Appl. Geophys.* **127**, 117–141.

THORPE, S. A. 2005 *The Turbulent Ocean*. Cambridge University Press.

WARD-SMITH, A. J. 1980 *Internal Fluid Flow – The Fluid Dynamics of Flow in Pipes and Ducts*. Oxford University Press, ISBN 0–19–856325–6.

WILLIS, G. E. & DEARDORFF, J. W. 1981 A laboratory study of dispersion from a source in the middle of the convectively mixed layer. *Atmos. Environ.* **15**, 109–117.

WILLIS, G. E. & DEARDORFF, J. W. 1983 On plume rise within a convective boundary layer. *Atmos. Environ.* **17**, 2435–2477.

WILLIS, G. E. & DEARDORFF, J. W. 1987 Buoyant plume dispersion and inversion entrapment in and above a laboratory mixed layer. *Atmos. Environ.* **21**, 1725–1735.